Journal of Volcanology and Geothermal Research 239–240 (2012) 83–91

Contents lists available at SciVerse ScienceDirect

Journal of Volcanology and Geothermal Research

journal homepage: www.elsevier.com/locate/jvolgeores

Seismic structure of the Tengchong volcanic area southwest China from local earthquake tomography

Yi Xu *, Xiaotao Yang [1], Zhiwei Li [2], Jianhua Liu [3]

Key Laboratory of Petroleum Resource Research, Institute of Geology and Geophysics, Chinese Academy of Sciences, P. O. Box 9825, Beijing 100029, China

ARTICLE INFO

Article history:
Received 22 March 2011
Accepted 12 June 2012
Available online 20 June 2012

Keywords:
Tengchong volcanoes
Seismic structure
Longling earthquake
Local tomography

ABSTRACT

We performed a local earthquake tomography to image the crust of the Tengchong volcanic area in southwestern China, using P-wave arrival data from a temporary network and permanent stations. The objective is to determine the magma sources of the volcanic area and the seismic structure of two M > 7 earthquakes in the Longling area south of Tengchong. The result reveals a correlation between the velocity structures and the volcanic activities from late Miocene to Holocene. A prominent low-velocity zone is observed beneath the central volcanic area, that is cored at 10–20 km depths and extends down to 30 km depth, with a lateral extent of 20–30 km. We infer that this unusual low-velocity zone represents a magma source of the heat flows for the volcanic eruption during Pleistocene and Holocene. Close to it, a high-velocity zone appears beneath the eastern volcanic area and it is likely to reflect solidified magma intrusions and high-density remnants within the cooled volcanic channel prior to Pleistocene. In the M > 7 earthquake area, the upper crustal structure shows evident variations across the Longling fault and the Nu River fault. Bounded by the two fault zones, the Gaoligong metamorphic belt and the Baoshan block are imaged by high velocities that are consistent with their high strength in the structures; on the contrary, low velocities are imaged in the area between the Longling fault and the Nu River fault, implying a decrease of the strength probably caused by igneous intrusions. It was the lateral variation in the rheologic structure that led to the uneven stress accumulations across these fault zones and created tectonic conditions for the seismic ruptures of the two M > 7 earthquakes in the Longling area.

1. Introduction

The Tengchong volcanic area is located in the southeastern Tibetan margin close to the China–Burma border (Fig. 1). About 70 volcanoes are distributed within a N–S trending rifting basin, which is bounded by the Sagaing fault to the west, by the Gaoligong fault to the east and by the Longling fault to the south. The Proterozoic to Paleozoic basement is broadly intruded by Mesozoic granites or overlain by Tertiary and Quaternary deposits (Jiang, 1998; Socquet and Pubellier, 2005; Wang et al., 2008). Most volcanic rocks are basaltic or andesitic and they are believed to be derived by the partial melting of enriched-mantle sources (Chen et al., 2002). Since late Miocene, volcanic eruptions had continuously occurred in the Tengchong area and their activities could be divided into several stages, with the latest eruptions in Holocene (Li et al., 2000; Wang et al., 2007; Zou et al., 2010). Prior to Pleistocene, most volcanic eruptions were concentrated on the eastern and western margins of the Tengchong basin; from Pleistocene to Holocene, they migrated into the Tengchong basin; at present, hydrothermal eruptions can be observed in hot springs of the central volcanic area (Shangguan et al., 2005). Geophysically, the volcanic area is characterized by high heat flows, high attenuation (low Q), low electrical resistivities and low seismic velocities (Qin et al., 2000; Bai et al., 2001; Lou et al., 2002; Wang and Huangfu, 2004). The low-velocity anomalies are distributed not only within the crust but into the upper mantle (Huang et al., 2002; Wang et al., 2003; Zhao, 2007; Lei et al., 2009). On May 29, 1976, two M > 7 earthquakes occurred in the Longling area south of Tengchong, which are attributed to displacements of the Longling fault and the Nu River fault (Wang et al., 2006).

The origin of the Tengchong volcanic is debated, including the subduction of the Burma microplate or the Indian plate (Huang et al., 2002; Zhao, 2007; Lei et al., 2009), the dextral strike-slip displacement of the Sagaing fault (Wang et al., 2007) or the assimilation of subducted slab of the oceanic crust or sediments of Neo-Tethyan basin (Chen et al., 2002). Although both geological and geophysical studies support the presence of magma chambers beneath the volcanic area, the geometry of the heat flow system is not well constrained; particularly, the relations between the crustal structures and the volcanic activities of different periods remain unclear. From Dec 2002 to Dec 2003, we deployed a temporary earthquake observation in western Yunnan, and installed more than 20 stations in Tengchong and surrounding area. Using the earthquake data from these stations and other permanent stations, we imaged the crust of the area between 97°–100°E and 24°–26°N, with

* Corresponding author. Tel./fax: +86 10 8299 8144.
E-mail addresses: xuyi@mail.iggcas.ac.cn (Y. Xu), xiaotaoyang@mail.iggcas.ac.cn (X. Yang), zwli@mail.iggcas.ac.cn (Z. Li), jhliu@mail.iggcas.ac.cn (J. Liu).
[1] Tel.: +86 10 8299 8145.
[2] Tel.: +86 10 8299 8104.
[3] Tel.: +86 10 8299 8145.

0377-0273/$ – see front matter © 2012 Elsevier B.V. All rights reserved.
doi:10.1016/j.jvolgeores.2012.06.017

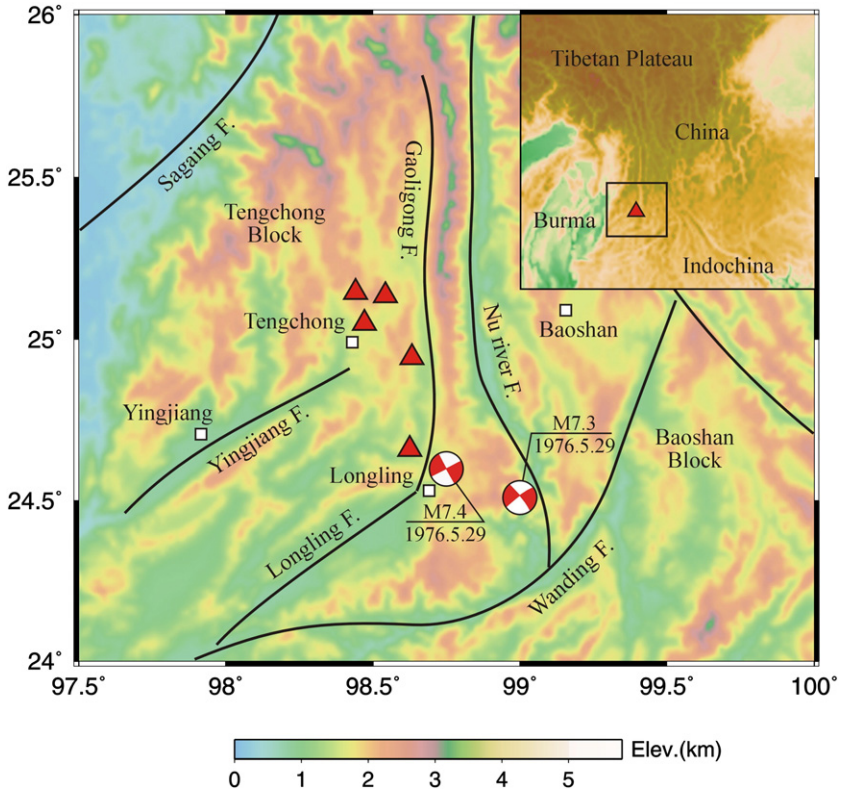

Fig. 1. Tectonic outline of the study area. Red triangles are main volcanic locations. Focal mechanisms are two M > 7.0 earthquakes on May 29, 1976 (derived from the Harvard Global CMT Catalog). Their locations and magnitudes refer to the China National Earthquake Bulletins. Black solid lines are major active faults. The color scale bar denotes topography of the study area. Inset sub-figure is a large scale map showing the location of the study area.

objectives to refine the seismic structure of the Tengchong volcanoes and the Longling Ms > 7 earthquake area.

2. Data selection

The data used in this study are P-wave arrival times from local earthquakes recorded by the temporary network and eight permanent stations in the study area (Fig. 2). The temporary network consisted of 24 broadband stations equipped with the RefTek Digital Acquisition Systems (DAS) and three-component seismometers (Guralp CMG-3ESP). Recording was continuous at 50 samples per second and timing was controlled by the Global Position System. The eight permanent stations belong to the Yunnan Earthquake Network that began to operate from 1970. Early permanent stations were equipped with short-period seismometers; after 2001, most of them were replaced with broadband seismometers and timing services were updated from quartz clocks to the global position system. P- and S-wave phases of the earthquakes were picked from three-component seismograms. Their arrival times were compiled into local earthquake bulletins.

We firstly selected earthquake waveforms from recording data of the temporary stations, according to local earthquake catalogues. All events were required to be located within the temporary network and to have impulsive P-wave arrivals. Arrival times of the selected events were picked from the vertical components of the digital seismograms and reading uncertainties of the impulsive phases were about 0.02 s. We only considered those events with clear phases and sufficient observations to ensure the quality of earthquake relocations. The dataset included 1578 P-wave arrivals from 106 events; in general, their magnitudes were limited to be above M1.5–2.0. Since the data from the temporary stations could not provide sufficiently dense ray path coverage, we supplemented additional data from the local earthquake bulletins. They included 4471 P-wave arrivals from 1494 events that occurred during 1990–2009 and were recorded by the permanent stations in the study area. Source parameters of these events had been determined using P- and S-wave arrival data from all recording stations in the Yunnan Earthquake Network. The estimated uncertainties of the event locations were generally less than few kilometers. In this study, we made two efforts to decrease the uncertainties of the event locations. The first was to preclude those events with unusual travel time residuals that were brought by incorrect source parameters rather than arrival readings. This process required careful analysis of the travel time residuals for each event. The second was to relocate the events through an iterative inversion like that in many tomographic studies, but the quality still depends on the geometry of the station distributions. After the inversion, we notice some improvements in the event locations, but most of them are located in the area covered by the temporary stations, because they have more observations for the earthquake relocation.

To avoid earthquake clusters, we followed the technique of Liang et al. (2004) to optimize the data coverage of the study area. The basic idea is to select the event with most observations in a cluster with a given radius and to discard other events in that cluster. This procedure can reduce the degree of the unevenness in the earthquake distributions but still keeps the overall ray path coverage. After comparing with different values, we chose 4.5 km as the radius of the event cluster. Finally, we obtained 2870 arrivals from 593 events, most of which occurred in the upper-middle crust above 30 km depth. All arrival data were required to have travel time residuals of less than ± 2.0 s (Fig. 3). The data shows good ray path coverage in the volcanic area (Fig. 2).

3. Model description

We constructed a preliminary 1-D model based on a seismic sounding profile across the Tengchong volcanic area (Wang et al.,

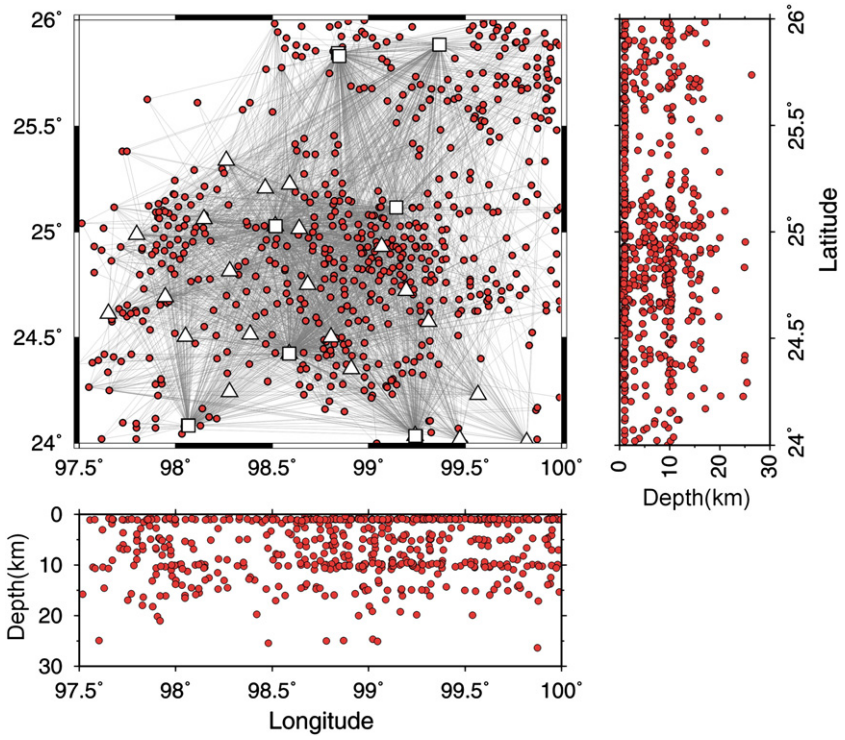

Fig. 2. Locations of temporary stations (white triangles), permanent stations (white squares) and earthquake sources (red circles) in the study area. Gray lines denote the ray paths between the earthquake sources and the recording stations. Two maps along latitude and longitude are hypocenters projection at depths.

2003). In this model, the crust is divided into seven layers between 1 km, 4 km, 8 km, 12 km, 17 km, 23 km and 43 km depths with increasing thickness intervals in the vertical direction. P-wave velocities at these depths are derived from those at corresponding depths on the seismic sounding profile; the average crustal thickness (43 km) is correspondent to the Moho depth in the Tengchong area determined from the tele-seismic receiver function and seismic sounding studies (Wang et al., 2003; Gao et al., 2009). Actually, as the ray paths of the study area are mostly distributed within the crust, the ray tracing will not be affected by the variation of the Moho depth. Beneath the Moho, the uppermost mantle is divided into two layers between 43–50 km depths and 50–77.5 km depths. P-wave velocity at 77.5 km depth is derived from the global model AK135 and that at 50 km depth is calculated through interpolation. The base of the model volume is fixed at 77.5 km depth. We gridded the volume model along latitude and longitude, according to the present data coverage. After testing different grid sizes, the resolution estimate suggested that the model volume could be meshed by a set of $0.2^\circ \times 0.2^\circ$ grid cells, totally including 1936 grid node parameters for the velocity inversion.

To fit the arrival data, we modified the preliminary model through the inversion. In the first step, based on the preliminary model, the arrival times were inverted to obtain a 3-D model that includes lateral variations in actual structures. From it we got a depth-averaged model (Intermediate model M1). Then, the M1 model was applied to the next inversion as the input model; in a similar way, we obtained the second depth-averaged model (intermediate model M2). Compared to the preliminary model, the M1 model shows small changes at given depths, but these changes become evident in the M2 model, in which velocities are slower at 4–13 km depths and at 30–43 km depths, but faster at 17–23 km depths (Fig. 4). Further comparison indicates that the M2 model is much close to the depth-averaged model derived from final result of the actual inversion. Thus, we determined to use the M2 model as the starting model of the actual inversion.

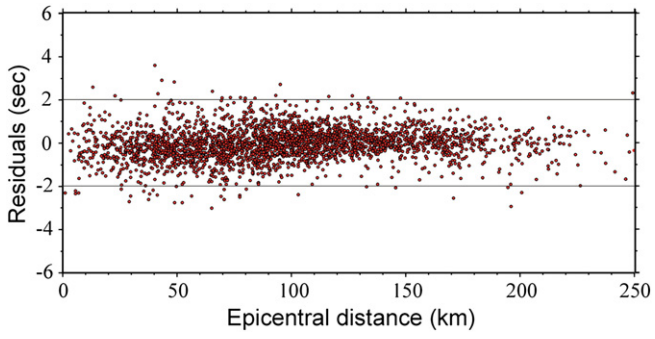

Fig. 3. Distribution of travel time residuals versus epicentral distance. The time residuals are required to be less than ±2.0 s in this study.

4. Inversion procedure

The 3-D ray tracing procedure was used to calculate synthetic travel times from the earthquake sources to the recording stations in the model volume (Zhao et al., 1992; Koketsu and Sekine, 1998), in which station elevations were taken into account. We jointly inverted the source locations and the velocity parameters through the damped LSQR algorithm (Paige and Saunders, 1982) and iterative process. The first iteration was performed based on the 1-D starting model (M2) and original source parameters. The output result included modification of the source parameters and a 3-D model that have lateral variations in actual structures. In the next iterations, using the modified source parameters, the travel times were recalculated through the ray-tracing procedure in the current 3-D model, until a small model variance was approached.

Figs. 5 and 6 illustrate the variation of the RMS versus iteration numbers and the residual distribution before and after the inversion. For the joint inversion, the RMS rapidly decreases after three iterations;

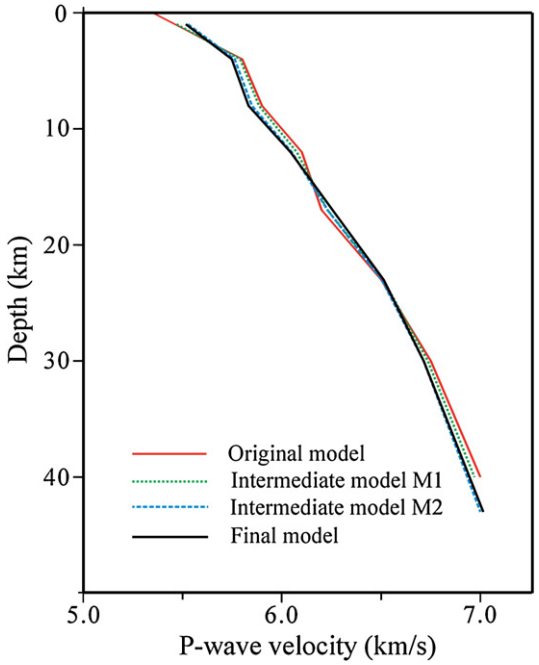

Fig. 4. 1-D velocity models used in this study. The red solid line is the preliminary model derived from a deep seismic sounding profile (Wang et al., 2003); the green and blue dashed lines are two intermediate models (M1 and M2); the black solid line is the depth-averaged model from the final result of actual inversion.

for the earthquake relocation, the RMS decreases after two iterations, but increases smoothly later. Considering the trade-off between them, we choose the output model of the second iteration for tectonic analysis. We note that the RMS of the joint inversion and earthquake relocation varies within small ranges. One reason is that the refined starting model (M2) is much approaching to the actual structure of the study area; it is also determined by the data quality and structural variations.

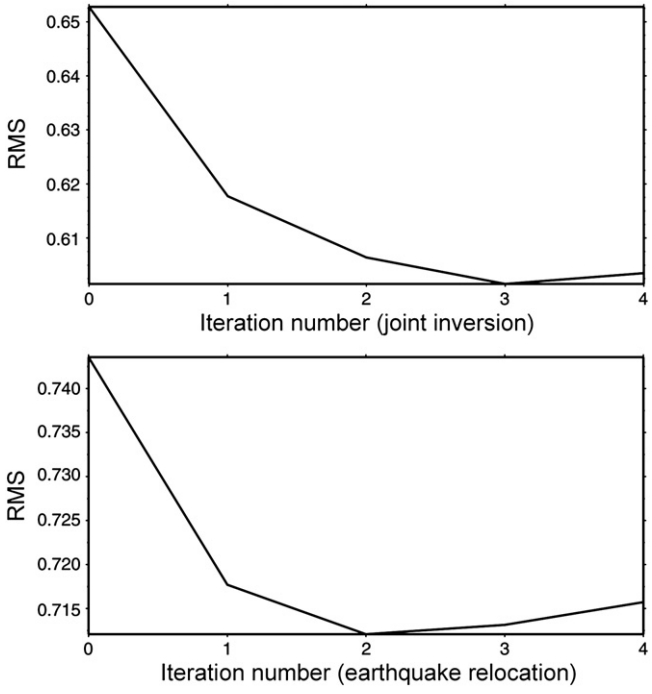

Fig. 5. The variance of the RMS versus iteration numbers for the joint inversion (upper) and the earthquake relocation (lower).

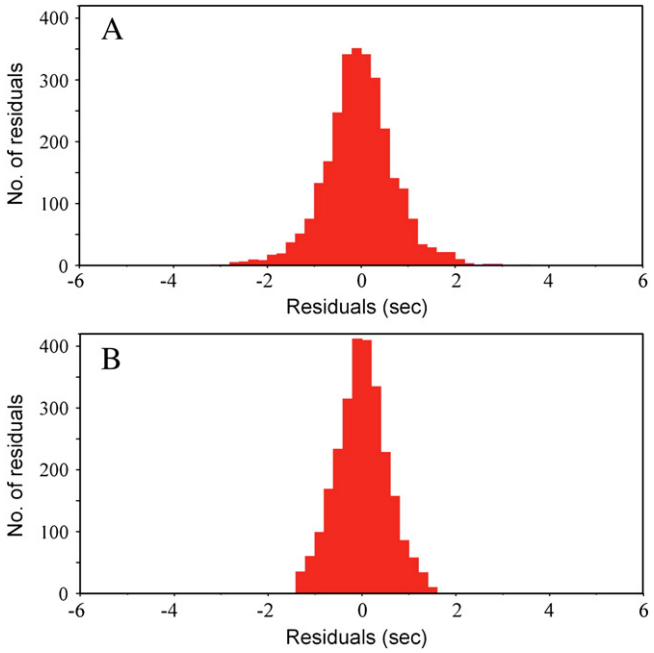

Fig. 6. Histograms of the travel time residuals before (upper) and after (lower) the inversion.

Since data outliers and unevenness of ray paths tend to make the linear equation system inconsistent, we followed the technique of Lees and Crosson (1989) to use the Laplacian operator as smoothness constraints to control unreasonable local anomalies in the inversion.

5. Resolution test

The checkerboard test was performed to examine model resolutions. The input model consisted of a set of alternating positive and negative perturbations with the maximal amplitude of 5% relative to the P-wave velocities in the starting model (M2). Real source-station pairs were used to calculate synthetic travel times within the model volume. Then, the synthetic data were inverted by using the same procedure as that for the real data to recover the input model. In order to analyze the resolution, we compare the recovered model with the known synthetic model to examine what can be reconstructed. The recovered checkerboard patterns in Fig. 7A indicate that the most parts of the input model can be resolved using the $0.2^\circ \times 0.2^\circ$ grid cells except the far corners, because of better sampling of the crossing ray paths beneath the network.

We also performed a spike test to examine the model resolution in the Tengchong volcanic area. The synthetic spike is located at 8–23 km depths beneath the center of the volcanic area and its lateral extents are about 50 km × 50 km. The spike is defined by a negative velocity anomaly of 5% over the background velocities of the starting model (M2). In the recovered model (Fig. 7B), we note that the synthetic spike is almost reconstructed, except the region below 23 km depth. This is due to few sources in the deep crust and hence the nodes are less sampled by crossing ray paths. In general, the degree of the recovery is acceptable for most parts of the study area and it is comparable with the data coverage shown in Fig. 2, indicating that our network geometry and the event distribution are adequate in resolving the upper-middle crust of the volcanic area.

6. Tomographic result

Map views in Fig. 8 illustrate P-wave velocity variations at 4–30 km depths, which are indicated by perturbations in percent relative to the velocities in the starting model (M2). The most prominent feature is

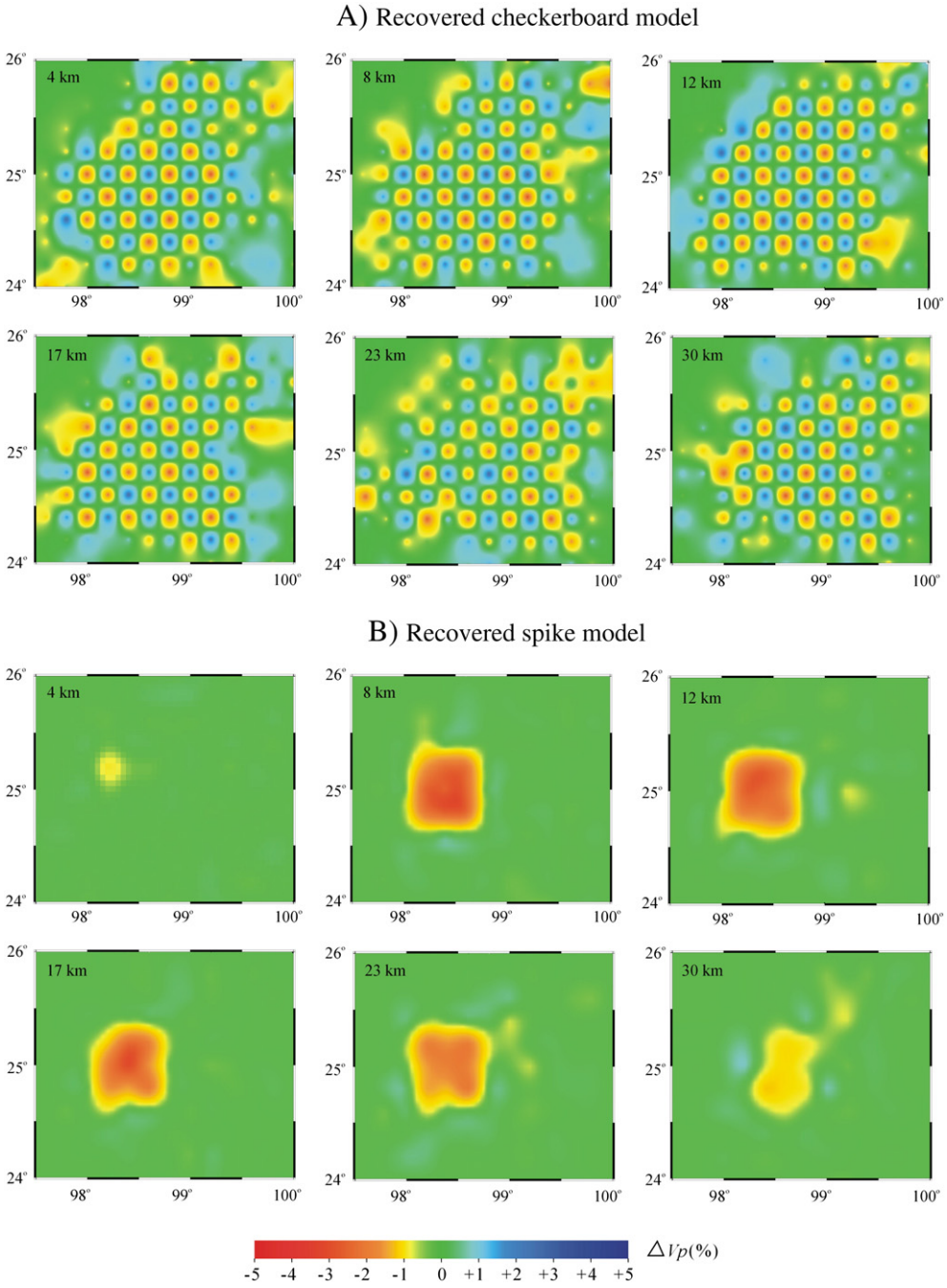

Fig. 7. Recovered checkerboard model (A) and synthetic spike model (B). The layer depth is shown on the top left corner of each map. For the checkerboard test, the input model consists of alternating positive and negative perturbations (in percent) with the maximal amplitude of 5% relative to the starting model (M2), and the grid cells are 0.2°×0.2°. For the spikes test, the synthetic spike is located at 8–23 km depths beneath the Tengchong area, with lateral extents of about 50 km×50 km. It is defined by a negative anomaly of 5% over the background velocities of the starting model (M2).

low-velocity anomalies beneath the Tengchong volcanoes, which are surrounded by high-velocity anomalies in adjacent areas. This feature is particularly clear at 12–30 km depths. At 4 km depth, low-velocity anomalies dominate most of the area between Tengchong and Longling; at 8 km depth, however, they are mainly concentrated between the Gaoligong fault and the Nu River fault.

Tomographic profiles in Fig. 9 illustrates P-wave velocity variations across the center of the Tengchong volcanic area (A-A, B-B, C-C and D-D) and the epicenters of the two M > 7.0 earthquakes in the Longling area (E-E). Their locations are shown by the 4-km map view in Fig. 8. There are evident velocity contrasts between the Tengchong volcanoes and surrounding area. The volcanic area is characterized by a prominent low-velocity zone (5.8–6.2 km/s), which is cored at 10–20 km depths and probably extends down to 30 km depth, with lateral extents of 20–30 km. This low-velocity zone is overlain by a thin normal-velocity layer and doesn't link the near-surface low-velocity layer. Besides, the structure of the volcanic area is symmetric in the north–south direction (profile A-A), in which the low-velocity zone is bounded by the normal velocities to the north and the south. In the east–west direction (profile B-B), however, a high velocity zone appears beneath the eastern volcanic area and its depth ranges between 5 and 15 km. There are few earthquakes in the low-velocity zone beneath the volcanic area and they are mostly distributed around the top of the eastern high-velocity zone.

Strong velocity variations are observed in the upper crust above 12 km depth across the Gaoligong fault and the Nu River fault. Both

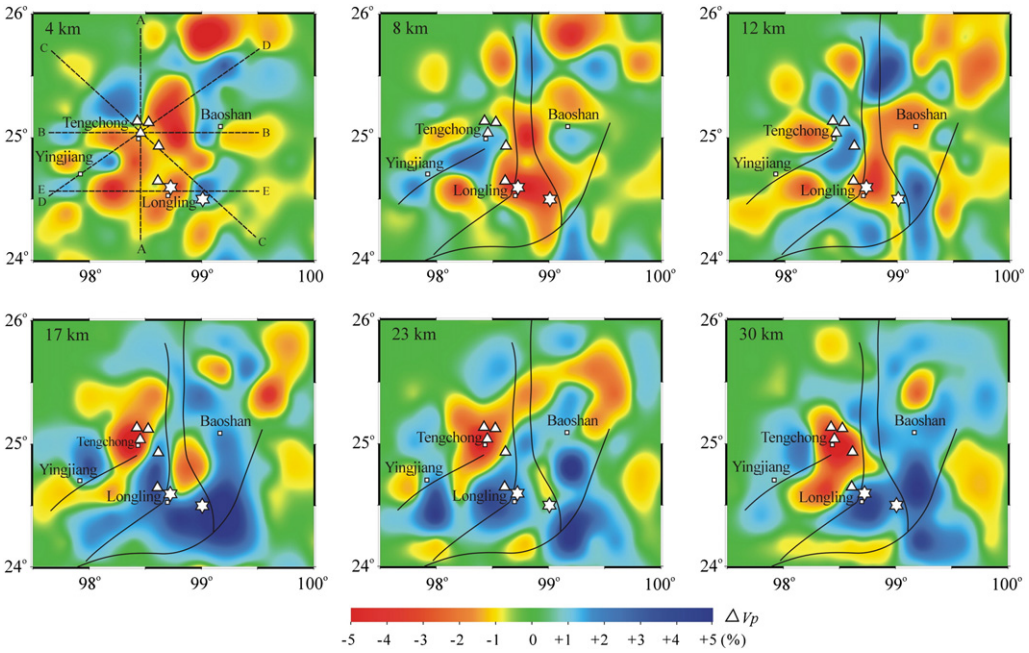

Fig. 8. Map views of P-wave velocities at 4–30 km depths. The velocity images are indicated by perturbations in percent relative to the starting model (M2). The layer depth is shown in the top left corner of each map. Locations of the main volcanoes (white triangles), M > 7.0 earthquakes (white hexagon stars) and active faults (black line) are the same as those in Fig. 1.

of the two fault zones appear as gradient belts between high and low velocities. The earthquakes near the fault zones are almost located at 0–20 km depths. Locations of the two M > 7.0 earthquakes in the Longling area are associated with the upper crustal variation across the Nu River fault and Longling fault (Profile E-E in Fig. 9). Compared to the high velocities in the eastern and western sides (5.6–6.0 km/s), the area between the two fault zones has very low velocities (<5.6 km/s). This low-velocity zone extends to 10–12 km depths, and many earthquakes are distributed around adjacent gradient belts, including the M7.4 earthquake near the Longling fault and the M7.3 earthquake near the Nu River fault. We infer that the two M > 7.0 earthquakes occurred at the roots of the gradient belts.

7. Discussion

7.1. Comparison with previous studies

Many geophysical studies focus on the seismic structure of the Tengchong volcanic area. In a local tomographic study, Qin et al. (2000) noticed two low-velocity anomalies at 3–9 km and 15–24 km depths beneath the Tengchong area and attributed them to the magma chambers associated with the melt accumulation. In a magnetotelluric study south of Tengchong, Bai et al. (2001) outlined a dome-like conductive structure (<30 Ωm) at 5–25 km depths and related it to a potential magma reservoir beneath the Rehai geothermal field. Seismic sounding studies by Lou et al. (2002) and Wang and Huangfu (2004) revealed a low-velocity zone in the upper crust south of Tengchong and it is suggested to reflect the geothermal activity and magma differentiation derived from the upper mantle. Tele-seismic receiver function studies by Wang and Huangfu (2004), He et al. (2004) and Gao et al. (2009) verified the unusual low velocities at 10–20 km depths beneath the Tengchong area. By analyzing relative geothermal gradients, Zhao et al. (2006) inferred that the volcanic area is underlain by three magma chambers that have lateral extents of 19–28 km and are located at 4–27 km depths. Tomographic studies in southwestern China also revealed the low-velocity anomalies associated with the magma activities in the upper crust of the Tengchong area (Huang et al., 2002; Wang et al., 2003; Zhao, 2007; Lei et al., 2009). These studies reflected the basic features of the volcanic area, including low seismic velocities, low electric resistivities and high heat flows. However, we still need more constraints on the detailed structures of the magma system, such as numbers of magma sources, their depth ranges and lateral extents. These uncertainties can be attributed to the differences in the research methods, datasets, inversion models and resolution scales. Compared to previous studies based on the sparsely-distributed permanent stations, our study supplemented the arrival data from the dense high-quality temporary stations to increase the sampling of the crossing ray paths beneath the study area. These data largely improved the degree of the resolution in the Tengchong volcanic area. As shown in Figs. 8 and 9, our result not only reflects the low-velocity feature of the volcanic area, but places better constraints on lateral and vertical variation of the volcanic structures.

7.2. The magma system for the volcanic area

In general, low-velocity anomalies beneath volcanoes are interpreted as evidence for the melt accumulation in magma chambers, whereas high-velocity anomalies represent extinct magma bodies or older remnant magma systems that had cooled or solidified (Lees, 2007). In our result, the most considerable anomaly that is associated with the melt accumulation is the prominent low-velocity zone beneath the Tengchong basin, which represents an unsolidified magma source or a heat flow channel of the volcanic area. A qualitative estimate indicates that this magma source is cored at 10–20 km depths and has a lateral extent of 20–30 km. It links deep sources through heat flow channels within the lower crust. This estimate is approximate to the magma source inferred by Qin et al. (2000) from the local earthquake tomography and to the magma reservoir inferred by Bai et al. (2001) from the magnetotelluric survey, but different appreciably from those estimated by Lou et al. (2002) and Wang and Huangfu (2004) from the seismic sounding studies, in which the magma sources were considered to be located in the uppermost crust of above 10 km depth.

Low-velocity anomalies still appear at 4 km depth, but they are not only distributed in the Tengchong area, but also in other area east and south of Tengchong (Fig. 8). The profiles in Fig. 9 indicate that the near-surface low-velocity layer of the volcanic area is very thin and

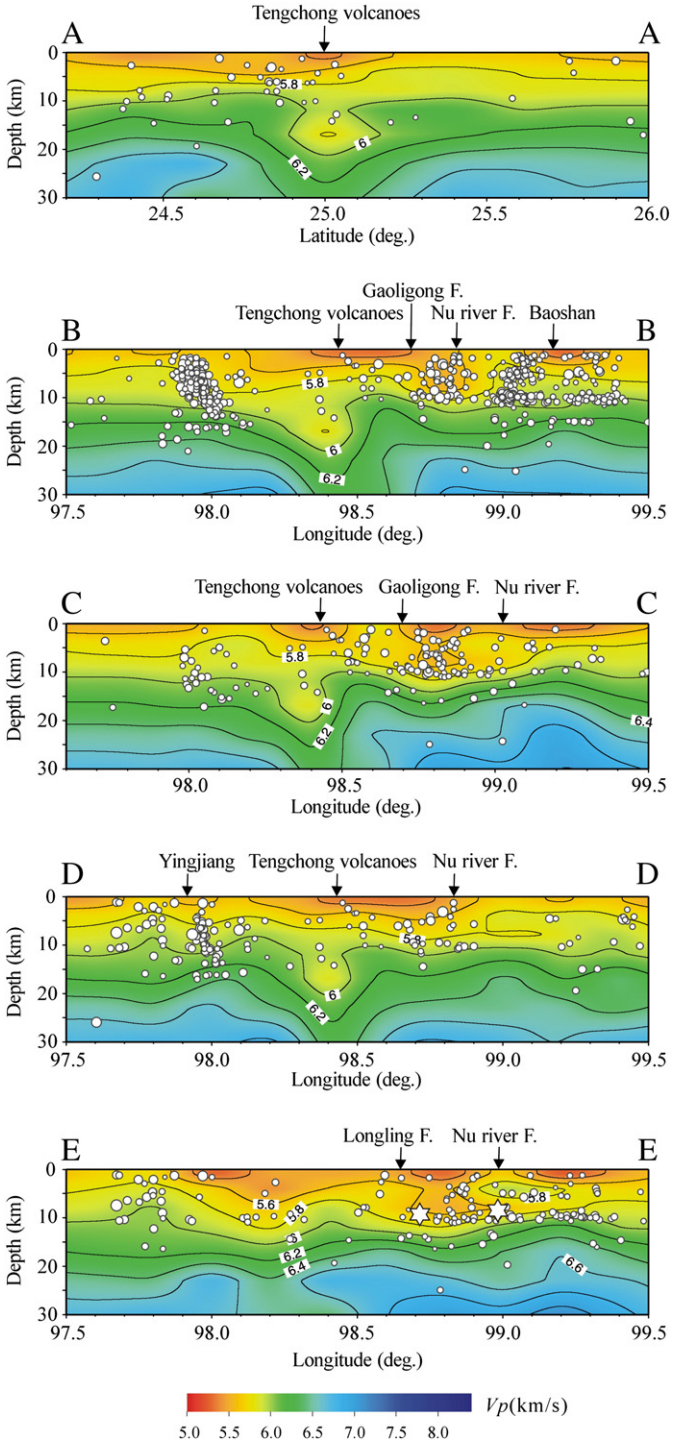

Fig. 9. P-wave velocity profiles across the central Tengchong volcanoes and the Longling M > 7.0 earthquake area. Their locations are showed by the 4-km map in Fig. 8. White circles are the relocated earthquakes near the profiles. White hexagon stars in the profile E-E are the M7.4 and M7.3 earthquakes, with estimated focal depths from this study. The color scale bar denotes the absolute velocities calculated from the velocity perturbations relative to the starting model (M2).

velocities are not very low. Its thickness and velocity anomalies are incomparable with the low-velocity zone at 10–30 km depths. We infer that these near-surface low-velocity anomalies are mainly caused by the Tertiary and Quaternary sediments, volcanic accumulations, fluid intrusions or hot springs within the Tengchong basin.

The seismic structures are correlated with the spatial and temporal variation of the volcanic activities. That is, the eastern Tengchong basin is underlain by the high-velocity zone that corresponds to early volcanic eruptions, whereas the central Tengchong basin is underlain by the prominent low-velocity zone that corresponds to late volcanic eruptions. Geological studies indicate that the volcanic eruptions in the Tengchong area tend to migrate from outside margins to the central basin from late Miocene to Holocene: prior to Pleistocene, they were concentrated in the southeastern Tengchong along the Lungchuan river; from Pleistocene to Holocene, they moved toward the Tengchong basin; the latest volcanic eruptions focused on three craters of the central basin (Li et al., 2000; Wang et al., 2007; Zou et al., 2010). In the eastern Tengchong basin, although early craters are not well preserved, volcanic rocks are widely outcropped along the Longchuan river and most of them are olivine-basalts; within the central Tengchong basin, some craters are well preserved and most volcanic rocks are andesites or andesite-basalts (Jiang, 1998).

As illustrated by a simplified model in Fig. 10, above correlation suggests that the low-velocity zone beneath the central Tengchong basin is associated with the volcanic eruptions from Pleistocene to Holocene, even to present-day high heat flow activities, whereas the high-velocity zone beneath the eastern Tengchong basin is likely to represent solidified magma intrusions or high-density remnants within cooled volcanic channels during late Miocene and Pliocene. Qin et al. (2000) also noticed the high-velocity anomalies at 10–15 km depths in the eastern Tengchong basin and attributed them to intrusive mafic rocks derived from the cooled mantle magma, but these high-velocity anomalies were not observed in the seismic sounding profiles (Lou et al., 2002; Wang and Huangfu, 2004) and other tomographic studies (Huang et al., 2002; Wang et al., 2003; Zhao, 2007; Lei et al., 2009). Structurally, current magma activities will continue to occur beneath the central Tengchong basin.

Although the estimated magma source is concentrated at 10–20 km depths and tends to extend down to 30 km depth, its transport system is probably linked to the partial melting or upwelling of the upper mantle in the western Yunnan and even to the lower crustal flow in the southeastern Tibet. There is a huge low-velocity anomaly beneath Tengchong area, that extends down to ~400 km depth and reflects the partial melting in the upper mantle (Zhao, 2007; Lei et al., 2009); while the lower crust of southwestern Yunnan is underlain by a 15–20 km thick low-velocity zone and it is interpreted as a weak zone of the lower crustal flow to decouple the upper crustal deformation from the underlying mantle (Gao et al., 2009). The lower crustal weak zone is also attested by the magnetotelluric study (Bai et al., 2010), in which two high-conductivity zones at 20–40 km depths are indicative of lower crustal flows around the eastern Tibet; the eastern zone is close to the Eastern Himalayas Syntax across the Tengchong area. Taken together, all these imply that the magma activities of the

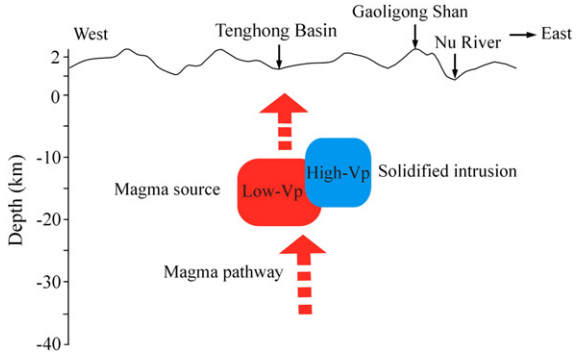

Fig. 10. Simplified model of the magma system of the Tengchong volcanic area. The western low-velocity body represents the magma source of the volcanic activities during Pleistocene and Holocene; the eastern high-velocity body reflects the solidified magma intrusion prior to Pleistocene.

volcanic area have deep background associated with the lower crustal flows and the partial melting or upwelling in the upper mantle. They provide geodynamic conditions for the magma generation and transportation.

7.3. The Longling M > 7.0 earthquakes

On May 29, 1976, two M > 7 earthquakes occurred in the Longling county south of Tengchong. According to source parameters in the China National Earthquake Bulletins, the first Ms 7.4 event is located close to the NE–SW trending Longling fault; the second Ms 7.3 event is located close to the N–S trending Nu River fault. Both of them are strike-slip events with steep fault planes (Harvard CMT Catalog). Due to a lack of geophysical data, seismic structures of the two events are rarely known. Their locations and focal depths have apparent uncertainties. For example, reported by the China National Earthquake Bulletins, they were located at 20–22 km depths; by the Harvard Mechanism Solutions, they were located at 15 km depth; based on a seismic sounding profile across western Yunnan, Zhang et al. (2005) inferred that the focal depths of the two events would be 10–12 km.

Geologically, the two Ms > 7 earthquakes occurred in a complicated tectonic area (Wang et al., 2008), which is bounded by the Longling fault to the west, by the Nu River fault to the east and by the Wanding fault to the south (Fig. 11). West of the Longling fault, the Gaoligong metamorphic belt is cored by the Paleozoic granites that intrude into the late Precambrian meta-sedimentary rocks; in the western part of the metamorphic belt, the granites are overlain by the Neogene sediments; toward the west, the Tengchong block is composed of the Proterozoic metamorphic rocks and late Paleozoic rocks, but the basement is widely intruded by the Mesozoic and Cenozoic granites. East of the Nu River fault, the Baoshan block is composed of the late Proterozoic to Mesozoic sediments and overlain by the Quaternary deposits; all rocks were involved in intensive shortening deformation along a number of N–S trending folds and thrust faults. The triangle area between the Longling fault and the Nu River fault is featured by a large amount of the Paleozoic and Mesozoic granites that intrude into the Proterozoic and Cambrian basement.

The velocity structure on the profile E–E reflects the variations of the rheologic strength in the upper crust of this area, that controls the stress accumulation across the Longling fault and the Nu River fault. The high-velocity features east of the Nu River fault and west of the Longling fault reveal a high strength upper crust of the Baoshan block and the Gaoligong metamorphic belt. This is consistent with the old rocks in the Precambrian basement that is available for the stress accumulation. The question is focused on the area between the Nu River fault and the Longling fault. Compared to the high velocities in neighboring areas, the lower velocities of this area imply a relatively weak (lower strength) upper crust. Likewise, the low velocities are also observed in the upper crust between the western Gaoligong metamorphic belt and the Yingjiang fault. A common feature of the two areas is that their basements are widely intruded by the Mesozoic granites. Therefore, one possible reason for the low-velocity feature between the Longling fault and the Nu River fault is that igneous intrusions destroyed the basement structures and hence decreased the rheologic strength of the upper crust. This inference is supported by a complicated fault system in this area, where many faults have remained active since Pleistocene (Wang et al., 2006) and they formed heat flow channels for the hot springs in the Longling area (Liao and Guo, 1986). Taken together, our analysis indicates that it was the variations in the rheologic structure that led to the uneven stress accumulations across the Longling fault and the Nu River fault. They created potential tectonic conditions for the seismic ruptures of the two M > 7.0 earthquakes in the Longling area. Based on the velocity gradients beneath the Longling fault and the Nu River fault, we estimate that the two events would occur at 10–12 km depths, similar to that inferred by Zhang et al. (2005) from the seismic sounding profiles.

8. Conclusion

Using P-wave arrival data from the temporary network and permanent stations, we performed a local earthquake tomography to image the seismic structures of the Tengchong volcanoes and the Longling Ms > 7 earthquake area in southwestern China. The result reveals a prominent low-velocity zone beneath the Tengchong volcanic area, that is cored at 10–20 km depths and extends down to

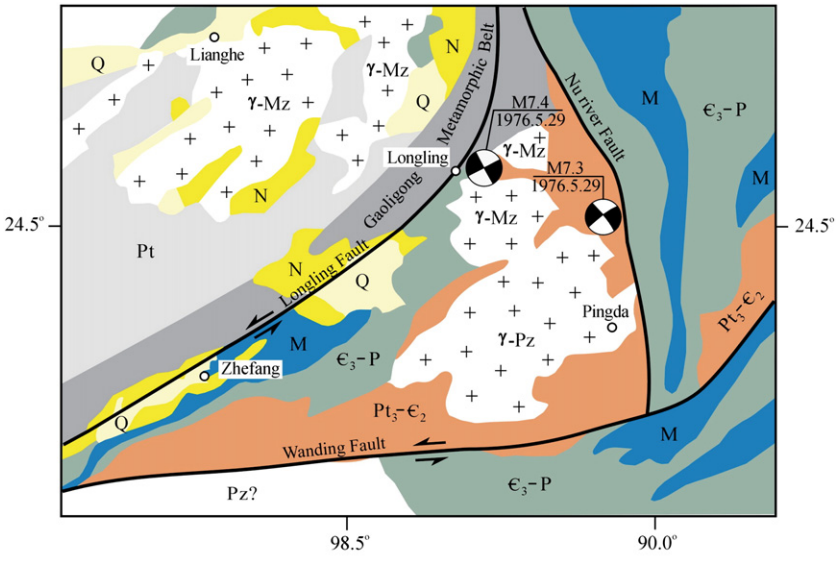

Fig. 11. Simplified geological map of the Longling area (Wang et al., 2008). Focal mechanisms are two M > 7.0 earthquakes on May 29 1976 (derived from the Harvard Global CMT Catalog). Their locations and magnitudes refer to the China National Earthquake Bulletins.

30 km depth, with the lateral extent of 20–30 km. We infer that it represents a magma source or a heat flow channel associated with the volcanic eruptions between Pleistocene and Holocene, whereas a relative high-velocity zone in the eastern volcanic area is likely to reflect solidified magma intrusions or high-density remnants within the cooled volcanic channel prior to Pleistocene. The occurrence of the two Ms > 7 earthquake south of Tengchong is related to the structural variations across the Longling fault and the Nu River fault. In the upper crust, the Gaoligong metamorphic belt and the western Baoshan block is imaged by the high velocities that reflect the high strength character of the basement structure, whereas the low-velocities are observed in the area between them, where the basement was widely intruded by the Mesozoic granites, suggesting a weakness in the structure. It was the strength variation in the rheologic structure that led to the uneven distribution of the stress accumulations across the Longling fault and the Nu River fault and created tectonic conditions for the seismic ruptures of the two M > 7.0 earthquakes in the Longling area.

Acknowledgment

This study was supported by the Natural Science Foundation of China (grant 40974027) and the China Geological Survey (BT-2008-04). We thank Prof. Fu Zhuwu of the Yunnan University for his assistance in the installation and maintenance of the temporary stations; we also thank technicians of the Yunnan Seismological Bureau for their help in data collection. We appreciate two reviewers for valuable comments and constructive suggestions.

References

Bai, D., Meju, M.A., Liao, Z., 2001. Magnetotelluric images of deep crustal structure of the Rehai geothermal field near Tengchong, southern China. Geophysical Journal International 147, 677–687.

Bai, D., Unsworth, M.J., Meju, M.A., Ma, X., Teng, J., Kong, X., Sun, Y., Sun, J., Wang, L., Jiang, C., Zhao, C., Xiao, P., Liu, M., 2010. Crustal deformation of the eastern Tibetan plateau revealed by magnetotelluric imaging. Nature Geosicence, http://dx.doi.org/10.1038/NGEO830.

Chen, F., Satir, M., Ji, J., Zhong, D., 2002. Nd–Sr–Pb isotopes of Tengchong Cenozoic volcanic rocks from western Yunnan, China: evidence for an enriched-mantle source. Journal of Asian Earth Sciences 21, 39–45.

Gao, X., Su, Y., Wang, W., Pei, S., Guo, Z., 2009. Lower-crust S-wave velocity beneath western Yunnan Province from waveform inversion of dense seismic observation. Terra Nova 21 (2), 105–110.

Harvard Global CMT Catalog, http://www.globalcmt.org/CMTsearch.html.

He, C.S., Wang, C.Y., Wu, J.P., 2004. S-wave velocity structure inferred from receiver function inversion in Tengchong volcanic area. Acta Seismological Sinica 26, 11–18 (in Chinese with English abstract).

Huang, J., Zhao, D., Zheng, S., 2002. Lithospheric structure and its relationship to seismic and volcanic activity in southwest China. Journal of Geophysical Research 107 (B10), 2255, http://dx.doi.org/10.1029/2000JB000137.

Jiang, C., 1998. Distribution characteristics of Tengchong volcano in the Cenozoic era. Journal of Seismology Research 21, 309–319 (in Chinese with English abstract).

Koketsu, K., Sekine, S., 1998. Pseudo-bending method for three-dimensional seismic ray tracing in a spherical earth with discontinuities. Geophysical Journal International 132, 339–346.

Lees, J.M., 2007. Seismic tomography of magmatic systems. Journal of Volcanology and Geothermal Research 167, 37–56.

Lees, J.M., Crosson, R.S., 1989. Tomographic inversion for three-dimensional velocity structure at Mount St. Helens using earthquake data. Journal of Geophysical Research 94, 5716–5728.

Lei, J., Zhao, D., Su, Y., 2009. Insight into the origin of the Tengchong intraplate volcano and seismotectonics in southwest China from local and teleseismic data. Journal of Geophysical Research 114, B05302, http://dx.doi.org/10.1029/2008JB005881.

Li, D., Li, Q., Chen, W., 2000. Volcanic activities in the Tengchong volcano area since Pliocene. Acta Petrological Sinica 16, 362–370 (in Chinese with English abstract).

Liang, C., Song, X., Huang, J., 2004. Tomographic inversion of Pn travel times in China. Journal of Geophysical Research 109, B11304, http://dx.doi.org/10.1029/2003JB002789.

Liao, Z.J., Guo, G.Y., 1986. Geology of the Tengchong geothermal field and surrounding area, west Yunnan, China. Geothermics 15, 339–345.

Lou, H., Wang, C., Huangfu, G., Qin, J., 2002. Three-dimensional seismic velocity tomography of the upper crust in Tengchong volcanic area, Yunan province. Acta Seismological Sinica 24, 243–251 (in Chinese with English abstract).

Paige, C.C., Saunders, M.A., 1982. LSQR: an algorithm for sparse linear equations and sparse least squares. ACM Transactions on Mathematical Software 8, 43–71.

Qin, J., Huangfu, G., Li, Q., Qian, X., Su, Y., Cai, M., 2000. 3-D chromatography of velocity structure in Tengchong volcano areas and nearby. Journal of Seismology Research 23, 157–165 (in Chinese with English abstract).

Shangguan, Z., Zhao, C., Li, H., Gao, Q., Sun, M., 2005. Evolution of hydrothermal explosions at Rehai geothermal field, Tengchong volcanic region, China. Geothermics 34, 518–526.

Socquet, A., Pubellier, M., 2005. Cenozoic deformation in western Yunnan (China–Myanmar border). Journal of Asian Earth Sciences 24, 495–515.

Wang, C.Y., Huangfu, G., 2004. Crustal structure in Tengchong volcano-geothermal area, western Yunnan, China. Tectonophysics 380, 69–87.

Wang, C.Y., Chan, W.W., Mooney, W.D., 2003. Three-dimensional velocity structure of crust and upper mantle in southwestern China and its tectonic implications. Journal of Geophysical Research 108, 2442, http://dx.doi.org/10.1029/2002JB001973.

Wang, J.N., Wang, Y.L., An, X.W., Yang, X.D., Chang, Z.F., 2006. Activity of the faults in the 1976 Longling M 7.3, 7.4 earthquake area. Journal of Seismology Research 29, 366–372 (in Chinese with English abstract).

Wang, Y., Zhang, X., Jiang, C., Wei, H., Wang, J., 2007. Tectonic controls on the late Miocene–Holocene volcanic eruptions of the Tengchong volcanic field along the southeastern margin of the Tibetan plateau. Journal of Asian Earth Sciences 30, 375–389.

Wang, G., Wan, J., Wang, E., Zheng, D., Li, F., 2008. Late Cenozoic to recent transtensional deformation across the Southern part of the Gaoligong shear zone between the Indian plate and SE margin of the Tibetan plateau and its tectonic origin. Tectonophysics 460, 1–20.

Zhang, Z., Bai, Z., Wang, C., Teng, J., Lu, Q., Li, J., Liu, Y., Liu, Z., 2005. The crustal structure under Sanjiang and its dynamic implications: revealed by seismic reflection/refraction profile between Zhefang and Binchuan, Yunnan. Science in China, Series D: Earth Sciences 48, 1329–1336.

Zhao, D., 2007. Seismic images under 60 hotspots: search for mantle plumes. Gondwana Research 12, 335–355.

Zhao, D., Hasegawa, A., Horiuchi, S., 1992. Tomographic imaging of P and S wave velocity structure beneath northeastern Japan. Journal of Geophysical Research 97, 19909–19928.

Zhao, C.P., Ran, H., Chen, K.H., 2006. Present-day magma chambers in Tengchong volcano area inferred from relative geothermal gradient. Acta Petrological Sinica 22, 1517–1528 (in Chinese with English abstract).

Zou, H., Fan, Q., Schmitt, A.K., Sui, J., 2010. U–Th dating of zircons from Holocene potassic andesites (Maanshan volcano, Tengchong, SE Tibetan Plateau) by depth profiling: time scales and nature of magma storage. Lithos 118, 202–210.